Lamb vector properties of swirling jets

W. Kollmann[1,2] **and G. Umont**[2]

[1]MAME Dept, University of Melbourne, Vic.3010, Australia

[2]MAE Dept, University of California Davis, CA 95616, USA

Abstract

Swirling jets show at Reynolds numbers in the transitional and low turbulence regime several competing flow forms due to shear and centrifugal instabilities. The swirling flow in jets at swirl numbers high enough to generate breakdown bubbles is simulated numerically using an accurate Navier-Stokes solver in cylindrical coordinates. The vector lines for vorticity and the Lamb vector are computed and analyzed in detail. The main result is that the set of critical points of the Lamb vector field contains stable and unstable manifolds characterizing high shear regions.

Introduction

The interpretation of flow fields can be guided by vector lines associated with vector properties of the flow. It is well known that streamlines, pathlines and streaklines generated by the velocity field give a unique picture of a steady flow, but differ significantly for unsteady flows as simple examples show (Hama, [1]). Turbulent flows are always unsteady and it is important to study vector lines generated by a variety of vector fields to gain an understanding of the kinematics and the dynamics of the flow. Velocity, vorticity and Lamb vector fields in axisymmetric, swirling jets are considered for this purpose with the emphasis on the Lamb vector. The Lamb vector is the cross product of vorticity and velocity and is, therefore, an indicator of regions of a flow field where vorticity is nonzero. It shares with velocity and vorticity critical points, but possesses additional critical points where the flow is locally Beltrami, i.e. a pure corkscrew motion.

Swirling jets show at Reynolds numbers in the transitional and low turbulence regime several competing flow forms due to shear and centrifugal instabilities ([3], [5], [4]). The swirling flow in jets at supercritical swirl numbers generating breakdown bubbles is simulated numerically using a hybrid spectral - finite difference method for the solution of the Navier-Stokes solver in cylindrical coordinates. The vector lines for vorticity and the Lamb vector are generated for this flow and analyzed in detail.

Numerical Method

The hybrid spectral finite-difference method developed in [6] is applied to solve the Navier-Stokes equations in cylindrical coordinates. The details including the verification of its accuracy and convergence properties are presented in [6] and [7]. The method takes advantage of the fact that smooth functions are periodic with respect to azimuthal variable and the discrete Fourier transform [8] is applicable, which is for axi-symmetric flows reduced to a single mode. The axial and radial directions are discretized using finite difference methods with formal accuracy at inner points up to 8th order. The time integrator is an explicit 4th-order state space Runge-Kutta method that requires minimal storage (see [6]). The Poisson/Helmholtz equations for streamfunction and pressure modes (see for [6] details) are solved using LU-decomposition (LINPACK, see Dongarra et al.[9]) combined with deferred corrections for bandwidth reduction.

Evolution of vector lines

The vector lines associated with vorticity and the Lamb vector are used as indicators for the variation of the swirling jet flow with time and the change of boundary conditions. The properties of the Lamb vector are discussed first.

Properties of the Lamb vector

The Lamb vector is defined as the cross product of velocity and vorticity

$$\mathbf{L} \equiv \mathbf{v} \times \nabla \times \mathbf{v} \tag{1}$$

It has interesting properties that can be exploited for the analysis of recirculation zones. The notion of the critical structure of the Lamb vector field is helpful for this analysis. It is defined as the set of points where $\mathbf{L} = 0$ and all stable and unstable manifolds intersected with the hull of the support of the vorticity field. The Lamb vector is trivially zero in irrotational zones, hence these regions are excluded. It will be shown that the critical structure of the Lamb vector field is particularly well suited for the detection of shear layers.

It is easy to show that the momentum balance for incompressible fluids can be rearranged in terms of vorticity. It emerges in the Lamb-Gromeka form as (the volume force is assumed to have a potential Φ)

$$\frac{\partial v_\alpha}{\partial t} - L_\alpha = -\frac{\partial}{\partial x_\alpha}(\frac{1}{2}v_\beta v_\beta + \frac{p}{\rho} + \Phi) - \frac{1}{Re}\varepsilon_{\alpha\beta\gamma}\frac{\partial \omega_\gamma}{\partial x_\beta} \tag{2}$$

This form of the momentum balance shows that viscosity has no influence on momentum transport if vorticity is zero, the viscous term is the curl of vorticity which is called flexion vector (Truesdell [2]). The left side of (2) is not acceleration since the gradient part of the convective acceleration is combined with the pressure and the potential of the volume force. If vorticity is zero, it follows from the Stokes theorem that velocity has also a potential and (2) leads to a Bernoulli theorem [2].

The Lamb-Gromeka form of momentum balance (2) contains the Lamb vector (1) representing the rotational part of the convective acceleration in the sense that the curl of the convective acceleration is equal to the curl of the Lamb vector. The Lamb vector furnishes a geometric interpretation of the case of steady inviscid flow with nonzero vorticity. The momentum balance (2) emerges then in the form

$$\nabla H = \mathbf{L} \tag{3}$$

where H denotes the Bernoulli head

$$H = \frac{1}{2}v_\beta v_\beta + \frac{p}{\rho} + \Phi \tag{4}$$

Equation (3) can be interpreted as follows: The gradient of H is in the direction normal to the surface formed by streamlines and vortex lines. This surface has the Lamb vector as normal vector and is called Lamb surface. It follows that the gradient has only one nonzero component normal to the Lamb surface
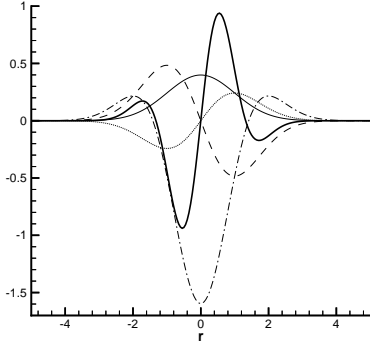
Figure 1: Velocity (v_θ dashed line, v_z thin full line), vorticity (Ω_θ dotted line, Ω_z dot-dashed line) and the Lamb vector component L_r (thick full line) for the swirling column example ($\sigma_\theta = \sigma_z = 1$, $S = 2$).

Figure 2: Detail of the Lamb vector lines at $t = 154.8$ for $Re = 2000$ and swirl number $S = 1.40$. The Lamb vector field is shown as red arrows

and we obtain the result that H=constant on the Lamb surface. This relation is satisfied for steady inviscid vortical flows and the Bernoulli head H depends in general on the particular Lamb surface chosen.

Further properties of the Lamb vector follow from the properties of velocity and vorticity. Elementary vector identities show that the Lamb vector can be represented by

$$L_\alpha = \frac{\partial}{\partial x_\alpha}\left(\frac{1}{2}v_\beta v_\beta\right) - v_\beta \frac{\partial v_\alpha}{\partial x_\beta} \tag{5}$$

This form can be seen as the difference between the gradient of the kinetic energy and the convective acceleration. The divergence of the Lamb vector is nonzero even for incompressible flows, given by

$$\frac{\partial L_\alpha}{\partial x_\alpha} = \omega_\alpha \omega_\alpha - \frac{\partial v_\alpha}{\partial x_\beta}\frac{\partial v_\alpha}{\partial x_\beta} + \frac{\partial^2}{\partial x_\alpha \partial x_\alpha}\left(\frac{1}{2}v_\beta v_\beta\right) \tag{6}$$

The example of linear Couette flow $v_1 = Ax_2$, $v_2 = v_3 = 0$ generates the divergence $\nabla \cdot \mathbf{L} = A^2$, where the Lamb vector is oriented in the positive x_2 direction $L_\alpha = \delta_{\alpha,2}A^2 x_2$. The Lamb vector field can be interpreted as the flow (regarding the Lamb vector as velocity) generated by a uniform distribution of sources with strength A^2. This vector field has the x_1-axis as unstable manifold.

The evolution of the Lamb vector is for incompressible Newtonian fluids governed by the pde

$$\frac{D\mathbf{L}}{Dt} = -\frac{1}{\rho}\omega \times \nabla p + \mathbf{v} \times (\omega \cdot \mathbf{s}) + \frac{1}{Re}\nabla^2 \mathbf{L} \tag{7}$$

(where $\mathbf{s} = \frac{1}{2}(\nabla \mathbf{v} + \nabla \mathbf{v}^T)$ denotes the rate of strain) which follows at once from mass and momentum balances. The Lamb vector is created or destroyed by two distinct processes. The first source term is the cross product of vorticity and the pressure gradient. It is zero if these two vectors are aligned and it is always present in plane flows. The second source is analogous to the vortex stretching term in the vorticity equation. It is easy to show that it is zero for plane flows and that it produces exponential growth in three-dimensional flows if the Lamb vector is aligned with the eigenvector of the rate of strain tensor associated with the middle (positive) eigenvalue. The critical structure of the Lamb vector field is a point set containing the
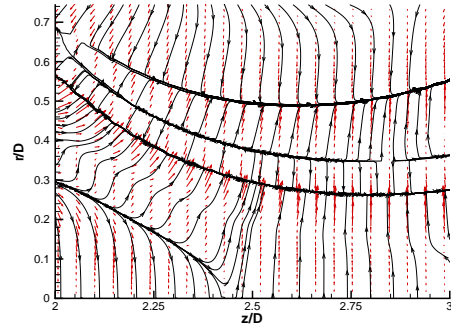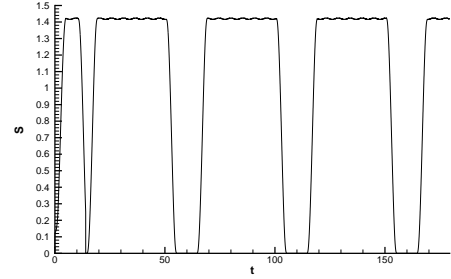
Figure 3: Swirl number as function of time for $Re = 2000$ and swirl number $S = 1.4$.
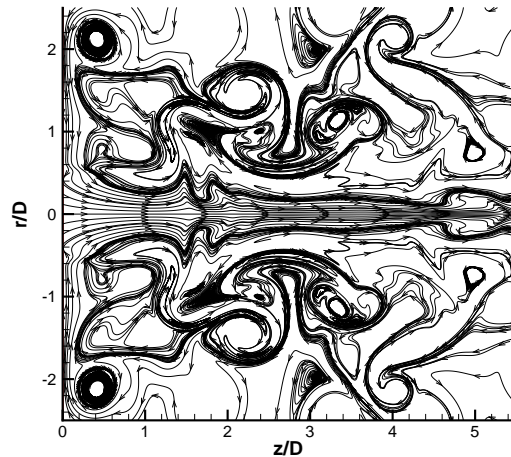
Figure 4: Vorticity lines at $t = 154.8$ for $Re = 2000$ and swirl number $S = 1.40$.
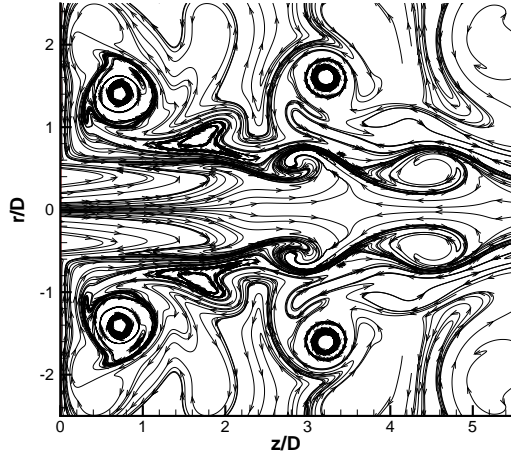
Figure 5: Vorticity lines at $t = 167$ for $Re = 2000$ and swirl number $S = 1.4$.

Figure 6: Lamb vector lines at $t = 154.8$ for $Re = 2000$ and swirl number $S = 1.4$.

critical point sets for velocity and vorticity as the definition (1) shows. In addition to the critical points for velocity and vorticity, Beltrami points, where velocity and vorticity are aligned, appear in the critical set of the Lamb vector.

Example for Lamb vector lines

The properties of the Lamb vector lines can be illustrated in an example. A swirling column of fluid is considered with velocity given in cylindrical coordinates by

$$v_r = 0, \quad v_\theta(r) = -\frac{rS}{\sigma_\theta^3 \sqrt{2\pi}} \exp\left(-\frac{r^2}{2\sigma_\theta^2}\right),$$

$$v_z(r) = \frac{1}{\sigma_z \sqrt{2\pi}} \exp\left(-\frac{r^2}{2\sigma_z^2}\right)$$

The vorticity components follow from their definitions at once

$$\Omega_r = 0, \quad \Omega_\theta(r) = \frac{r}{\sigma_z^3 \sqrt{2\pi}} \exp\left(-\frac{r^2}{2\sigma_z^2}\right),$$

$$\Omega_z(r) = -\frac{S}{\sigma_\theta^3 \sqrt{2\pi}} \left(2 - \frac{r^2}{\sigma_\theta^2}\right) \exp\left(-\frac{r^2}{2\sigma_\theta^2}\right)$$

The Lamb vector for this parallel flow has only one nonzero component

$$L_r = \frac{S^2}{\sigma_\theta^6 \sqrt{2\pi}} r \left(2 - \frac{r^2}{\sigma_\theta^2}\right) \exp\left(-\frac{r^2}{\sigma_\theta^2}\right) - \frac{r}{\sigma_z^4 \sqrt{2\pi}} \exp\left(-\frac{r^2}{\sigma_z^2}\right)$$

This implies that the radial locations where $L_r = 0$ (see the thick line in fig.1, which has apparently three roots) are in fact stagnation lines in the $r - z$ plane for the Lamb vector. In particular, the symmetry axis for axi-symmetric flows is in general stagnation line for the Lamb vector. The example indicates that two critical structures appear in a rotating fluid column: The center being an unstable manifold (line source) surrounded by a stable manifold (cylindrical surface). This is the situation that is emerging in the simulation of the swirling jet as shown in fig.6, 7 and in greater detail in fig.2. The details in the latter figure show the presence of several stable and unstable manifolds with the Lamb vectors as red arrows. The axis $r = 0$ changes from stable (sink) to unstable (source) with increasing z/D.

The Lamb vector lines away from the critical structure can be explained for regions where Bernoulli holds. Consider a streamline where the Bernoulli head H is constant, then is the Lamb vector parallel to the gradient of the Bernoulli head according to (3), hence orthogonal to the streamline. This is evident in fig.6, fig. 7 and fig.2.

Results for axi-symmetric flows

The simulation of axi-symmetric swirling jets were done for the Reynolds number Re defined by

$$Re \equiv \frac{v_z(0, z_0)D}{\nu} \tag{8}$$

the present results are for $Re = 2000$, and the swirl number S defined by Billant et al. [5] as

$$S \equiv \frac{2v_\theta(R/2, z_0)}{v_z(0, z_0)} \tag{9}$$

where $z_0 = 0.4D$ (D is the nozzle diameter), in the range $S = 1.0 - 1.45$, the present value is $S = 1.4$. The resolution was set to 121×251 gridpoints in radial and axial direction for the fourth order discretization of the non-convective spatial derivatives and the fifth order upwind-biased scheme for the convective terms. The entrance boundary conditions are a smooth top-hat profile for the axial velocity and a smooth profile for the azimuthal velocity with the maximum at $r/D = 0.25$. The entrance conditions were varied in time in cyclical fashion to follow the creation and destruction of the recirculation zones. The wind-down and wind-up phases of the entrance conditions are controlled with a C^∞-function (partition of unity) interpolating smoothly between the maximal and minimal values. The variation of the swirl with time at the entrance boundary is given in fig.3. Four wind-down and wind-up cycles are computed and the results are presented in terms of vector lines for vorticity and the Lamb vector.

Vector line results

The entrance boundary conditions for the azimuthal and the axial velocity are varied in time in a cyclical pattern to generate identical conditions with respect to the boundary conditions shifted by a finite time interval. The variation of the resulting swirl number (9) with time is given in fig.3. The third
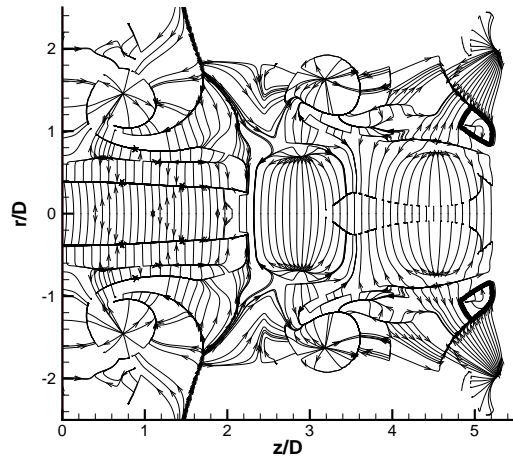
Figure 7: Lamb vector lines at $t = 167$ for $Re = 2000$ and swirl number $S = 1.4$.

and fourth cycle of wind-down and wind-up in the time intervals $[100, 120]$ and $[150, 170]$ are suitable for the structural investigation as the flow is sufficiently developed. The states at $t = 154.8$ and $t = 167$ are selected in the winding-down and winding-up phases of the fourth cycle, the two times correspond approximately to the same value of the Swirl number $S = 0.7$. The corresponding vector line pictures for the associated wind-down and wind-up states are presented in fig.4, fig. 6 at $t = 154.8$ (Vorticity lines) and fig.5, fig.7 at $t = 167$ (Lamb vector lines). The vortex lines in fig.4 and fig.5 in the subdomain $\mathcal{D}_1 \equiv [4, 5.2] \times [0, 1]$ show different connectedness, hence are topologically different in the two corresponding states.

The Lamb vector lines in fig.6 and fig.7 are in parts of the flow domain, where Bernoulli holds, orthogonal to the streamlines and possess critical points and stable and unstable manifolds where it does not hold. The manifolds are dominant and their number changes between the corresponding states of the flow. In particular, the subdomain $\mathcal{D}_1$ contains at $t = 154.8$ stable and unstable manifolds, which form a sorce point at the wind-up phase at $t = 167$. The core region in $0 \leq z \leq 2$ and $0 \leq r \leq 0.5$ at $t = 167$ forms a swirling column of fluid as presented in the example above.

Conclusions

The simulation of axi-symmetric swirling flows in jets at supercritical Swirl numbers shows that repeated self-similar variation of the entrance boundary conditions does not produce topologically equivalent flow states as measured by the vector lines of vorticity and the Lamb vector. The comparison of corresponding states in the down and upwinding phases produce critical structures which are topologically different. The Lamb vector lines possess stable and unstable manifolds indicating regions of high shear in addition to isolated critical points.

References

[1] Hama, F. (1962), "Streaklines in a perturbed shear flow", Physics of Fluids **5**, 644-650

[2] Truesdell, C.A. (1954), "The kinematics of vorticity", Indiana University Press, Bloomington, Indiana.

[3] Leibovich, S. (1978), "The structure of vortex breakdown", *Annual Rev. Fluid Mech. 10*, 221-246

[4] Shtern, V. and Hussain, F. (1998), "Instabilities of conical flows causing steady bifurcations", JFM *366*, 33-85

[5] P. Billant, J. Chomaz and P. Huerre (1999), "Experimental study of vortex breakdown in swirling jets", *J. Fluid Mech*, 376: 183-219.

[6] W. Kollmann and J.Y. Roy (2000), "Hybrid Navier-Stokes solver in cylindrical coordinates I: Method", Computational Fluid Dynamics Journal *9*, 1-16.

[7] W. Kollmann and J.Y. Roy (2000), "Hybrid Navier-Stokes solver in cylindrical coordinates II: Validation", Computational Fluid Dynamics Journal *9*, 17-22.

[8] Canuto, C., Hussaini, M.Y. and Zang, T.A. (1988), "Spectral Methods in Fluid Dynamics", Springer-Verlag, Berlin.

[9] J.J. Dongarra and C.B. Moler and J.R. Bunch and G.W. Stewart (1979), "LINPACK user's guide", SIAM Philadelphia